geosciences

MDPI

Article

Evaluating the Damping Ratio of Tailings by Different Experimental Methods: Case Study of Riotinto Mines

Hernán Patiño, Fausto Molina-Gómez, Rubén Ángel Galindo-Aires *

Department of Ground Engineering, Universidad Politécnica de Madrid, Calle Profesor Aranguren 3, 28040 Madrid, Spain; hernan.patino@upm.es (H.P.); fausto.molina@upm.es (F.M.-G.)
* Correspondence: rubenangel.galindo@upm.es

Abstract

Tailings are unconventional geomaterials that require dynamic characterisation due to seismic hazards at several storage facilities. Due to the anthropic origin of these materials, their dynamic properties differ from those reported for natural soils. In particular, the damping ratio is a relevant parameter that controls the dynamic response of tailings storage facilities. It can be estimated using different experimental methods. The objective of this research is to disclose the results obtained through laboratory tests in which the damping ratio was evaluated independently by Half-Power Bandwidth or the free-vibration decay methods. A comprehensive testing plan comprising resonant column tests and free-vibration decay tests was carried out on three types of tailings from the Riotinto mines (Huelva, Spain): Cerro Salomón Sand (CSS), High-Density Sludge (HDS), and Copper Lamas (CL). These tests were carried out under different effective consolidation pressures and torsional excitations. The results allowed the establishment of a series of relationships between the testing conditions and the identification of differences between the methods for tailings.

Keywords: dynamics; tailings; laboratory tests; modelling

1. Introduction

Research on the dynamic behaviour of soils has focused primarily on determining the shear modulus (G), with comparatively less attention devoted to evaluating the damping ratio (λ or D). Nevertheless, seminal studies by Hardin and Drnevich [1,2], Seed and Idriss [3], among others, have demonstrated that the damping ratio of soils is influenced by several factors, including the plasticity index (PI), effective consolidation pressure (σ_0'), level of induced angular strain (γ), void ratio (e), generated pore water pressure (u), and number of loading cycles (N).

Vucetic and Dobry [4], based on an extensive review of cyclic tests on clays with degree of over-consolidation (OCR) values between 1 and 8, showed that PI governs the variation in damping ratio with shear strain, particularly within the strain range $\gamma \approx 10^{-4}$ to 10^{-2}. At low strains, damping is relatively insensitive to PI, whereas at higher strains, soils with higher plasticity exhibit larger damping ratios. Further experimental work by Vucetic et al. [5], based on controlled-strain cyclic simple shear tests, confirmed that damping behaviour cannot be generalised across different clays. For comparable strain levels, some clays exhibited significant increases in damping with γ, whereas others showed limited or negligible variation. These differences were attributed to variations in soil fabric, stress history (e.g., OCR), and mineralogical composition. Zergoun and Vaid [6], using resonant column and cyclic triaxial tests on undisturbed Cloverdale clay, reported that for

Check for updates

Academic Editor: Meng Lu

Received: 9 March 2026
Revised: 13 April 2026
Accepted: 22 April 2026
Published: 26 April 2026

Copyright: © 2026 by the authors. Licensee MDPI, Basel, Switzerland. This article is an open access article distributed under the terms and conditions of the Creative Commons Attribution (CC BY) license.

cyclic stress ratios between 0.46 and 0.79, the damping ratio is practically independent of stress ratio. Brennan et al. [7], based on dynamic centrifuge tests on normally consolidated kaolinitic clay, found damping ratios up to 1.5 times greater than those measured in conventional laboratory tests, suggesting a strong frequency dependency.

Soriano et al. [8], using cyclic simple shear tests, examined the influence of pre-existing static shear stress (τ_o) combined with cyclic shear stress (τ_c) on the dynamic behaviour of saturated granular soils. Their results showed that, for a given number of cycles, the interaction between static and cyclic stresses significantly affects damping evolution. Patiño and Galindo [9] extended this approach to soft cohesive soils susceptible to sudden failure and demonstrated that the combination of monotonic and cyclic shear stresses controls the damping ratio. They proposed empirical relationships of the form $D(N, \gamma_c)$, $D(N, G/\sigma'_{ov})$ and $D(N, u/\sigma'_{ov})$ for different τ_o/σ'_{ov} ratios, as well as design charts for practical damping evaluation.

In granular materials, the damping ratio decreases with increasing confining pressure. Hardin and Drnevich [1] reported that the damping ratio of sandy soils decreases as a power function of the effective consolidation pressure, regardless of strain level. Kuribayashi et al. [10] found that the energy dissipation capacity of normalised Toyoura and Sengenyama sands decreases with increasing mean effective stress. Laird [11] showed that the minimum damping ratio of dry granular soils decreases with increasing effective confining pressure. Zhang et al. [12] demonstrated that both confining stress and geological age significantly influence damping ratio and, consequently, predicted spectral accelerations. Wichtmann and Triantafyllidis [13] showed that for quartzitic clean sands, the damping ratio and threshold strain levels are independent of the uniformity coefficient (C_u) and median grain size (D_{50}). Ham et al. [14] demonstrated that in dry clean sands, damping is more strongly affected by particle roundness and surface roughness than by sphericity. Madhusudhan and Kumar [15] found that increasing the degree of saturation from near-dry to fully saturated conditions produces only marginal increases in damping.

Numerous empirical correlations have been proposed to relate the damping ratio to controlling parameters in granular soils. Formulations were proposed by Hardin and Drnevich [1,2], Laird [11], Subramaniam et al. [16], Rollins et al. [17], Molina-Gómez et al. [18] and Patiño and Galindo [19], incorporating various combinations of shear strain, confining pressure, void ratio, soil gradation, number of cycles and pore water pressure.

Schaeffer et al. [20] demonstrated that damping ratios measured using free–free axial resonant column tests may be one to two orders of magnitude higher than those obtained from fixed–free torsional configurations in cohesive soils. Although damping is routinely employed in geotechnical dynamic analyses, relatively few studies have explicitly addressed the distinction between hysteretic and viscous damping mechanisms [21–23]. This limitation is particularly significant because different laboratory procedures, such as resonant column tests and free-vibration decay methods, capture different sources of energy dissipation. Consequently, damping values derived from these techniques are not always directly comparable. The authors of [21–23] primarily focused on conventional soils, highlighting that damping evaluation is highly dependent on both the testing methodology and the interpretation framework. However, this issue remains insufficiently explored for tailings materials.

This study aims to clarify the differences in damping ratios obtained through various experimental procedures in resonant column testing. To achieve this, an advanced experimental program using the resonant column apparatus on three different types of tailings from the Riotinto mines in Spain was conducted. The damping ratio was estimated using either the Half-Power Bandwidth method or the free-vibration decay method. As a result,

the empirical relationships proposed in this study are novel and provide valuable insights into the characterisation of damping ratios using different methodologies.

2. Materials and Methods

2.1. Materials

The materials used in this investigation were obtained from tailings deposits associated with the exploitation of the Riotinto mines, located in the central–eastern region of Huelva, Spain (Figure 1). The Riotinto mining district contains one of the most significant deposits of gold, copper and silver in Spain and has been exploited since approximately 2000 BC. Over centuries of mining activity, extensive waste dumps and tailings dams have been generated, currently occupying approximately 1200 hectares. These deposits are of considerable geotechnical interest, particularly in relation to the dynamic behaviour of tailings dams constructed using mining residues such as those examined in this study.

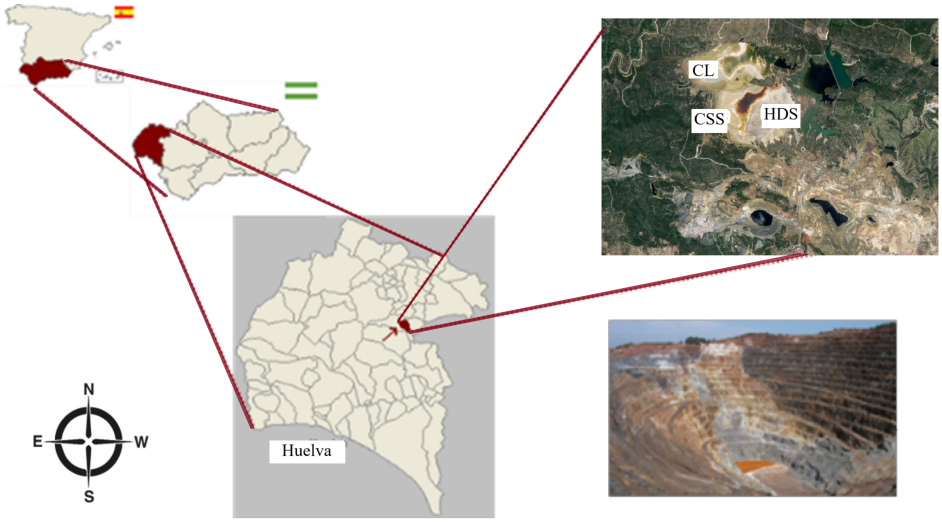


Figure 1. Location of Riotinto mines (adapted from [19]).

The samples were collected from the surface deposits in the tailings storage area, located at approximately 37°43′48″ N 6°35′16″ W. Three distinct materials were investigated, identified on site as Cerro Salomón Sand (CSS), High Density Sludge (HDS) and Copper Lamas (CL). The index properties of the tailings are summarised in Table 1.

Table 1. Index properties of the materials tested.

Material	In Situ Moisture (%)	Preparation Moisture (%)	<80 µm (%)	LL (%)	PL (%)	PI (%)	Specific Gravity	γ_d (g/cm^3)
CSS	8.1	8.1	32.7	–	–	NP	3.02	1.60
HDS	14.3	7.8	48.5	–	–	NP	2.99	1.65
CL	38.5	25.0	85.9	26.9	19.9	7	2.83	1.65

CSS and HDS are non-plastic materials (NP), whereas CL exhibits low plasticity with a plasticity index of 7%. The fine fraction (<80 µm) is significantly higher in CL, indicating a predominantly fine-grained structure compared with CSS and HDS materials. X-ray fluorescence analysis revealed that silicon, iron and sulphur are the dominant elements in all three materials, with corresponding oxides present in significant proportions. This mineralogical composition explains the relatively high specific gravity values reported in

Table 1. Detailed information on the mineralogical phases obtained from X-ray diffraction analysis is presented in Table 2.

Table 2. Mineralogical composition of the materials (%) [24].

Mineral Phase		CSS	HDS	CL
Quartz		92	82	23
Phyllosilicates	Chlorites	0	0	50
	Micas	8	6	17
Metallic minerals	Pyrite	0	0	9
	Jarosite	0	12	0

CSS and HDS are predominantly quartzitic materials, whereas CL contains a substantial proportion of phyllosilicates, particularly chlorites, as well as metallic minerals such as pyrite. The markedly different mineralogical compositions are expected to influence the mechanical and damping behaviour of the materials under dynamic loading.

2.2. Resonant-Column Testing and Damping Ratio Estimation

The resonant column apparatus used in this investigation was manufactured by Wykeham Farrance (Italy). This apparatus corresponds to a forced-vibration system with a single torsional degree of freedom, designed to induce vibration in the specimen over a frequency range encompassing its first natural mode. In the present study, specimens were fixed at the base and free at the top, corresponding to a fixed–free boundary condition (Figure 2). The excitation system incorporates an internal floating structure, allowing specimens to undergo significant axial deformation during consolidation without affecting the electronic components. Real-time visualisation of sensor responses is available throughout testing.

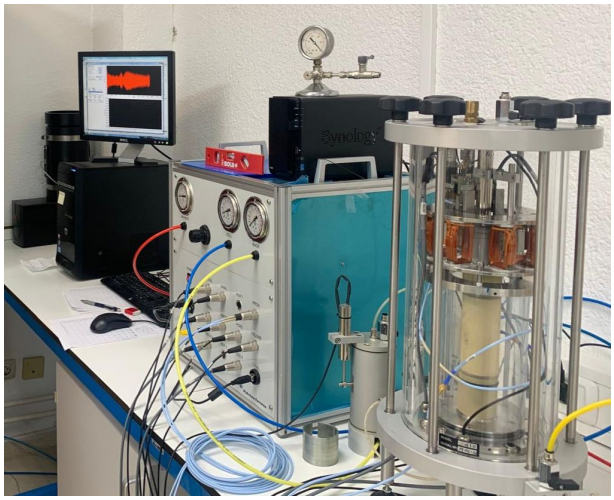


Figure 2. Photograph of the resonant -column apparatus of UPM.

The apparatus is fully automated and instrumented to estimate the resonant frequency, shear-wave velocity (V_s), shear modulus (G), angular strain, and damping ratio. This equipment allows for resonant column, cyclic torsional, and free-decay testing. In resonant column and free-decay modes, the equipment operates at frequencies typically greater than 10 Hz, whereas in cyclic torsional shear mode, the operating frequency is generally below 2 Hz. Control and data acquisition are performed through an integrated electronic unit comprising a power supply, manual and electronic pressure regulators, signal-conditioning modules and a computer interface. Therefore, no external signal generator or oscilloscope is required.

The damping ratio is evaluated using two independent procedures available in the resonant column apparatus, the Half-Power Bandwidth (*H-PB*) or the free-vibration decay (*F-VD*) methods. Both approaches assume that the soil specimen behaves as a single-degree-of-freedom torsional oscillator vibrating in its first mode. In this paper, λ is used to denote the damping ratio from the *H-PB* method, while the symbol D refers to the damping ratio of the *F-VD*. Figure 3 illustrates the fundamentals of these methods.

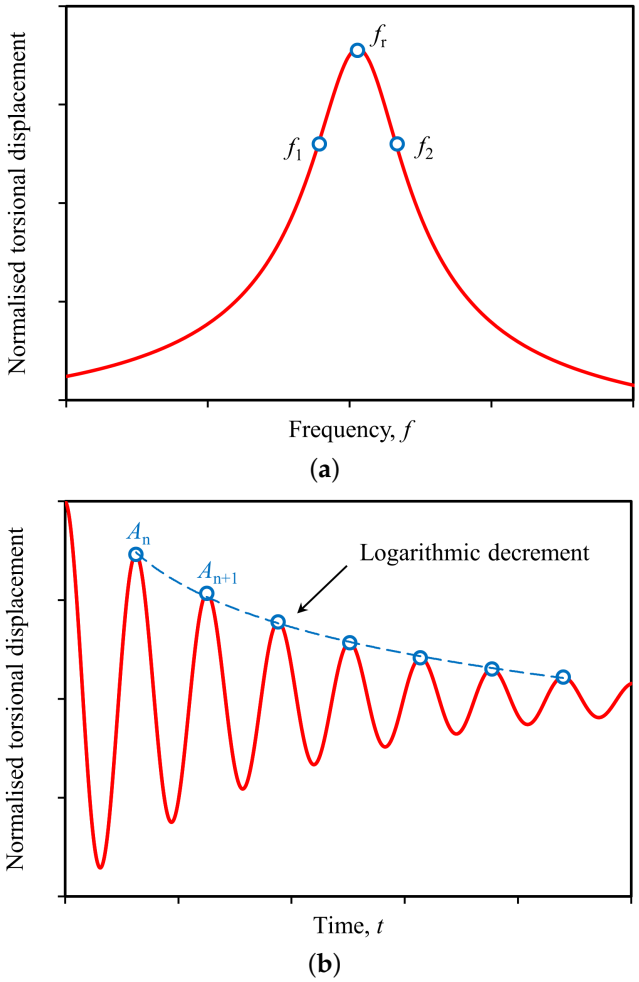


Figure 3. Methods to estimate the damping ratio: (**a**) Half-Power; (**b**) free-vibration decay.

In forced-vibration resonant column testing, the specimen is subjected to harmonic excitation over a range of frequencies until resonance is reached. The resonant frequency f_r corresponds to the frequency at which the amplitude of vibration is maximum. The damping ratio is obtained from the frequency response curve by identifying the two frequencies, f_1 and f_2, at which the vibration amplitude decreases to $1/\sqrt{2}$ of the maximum amplitude. These frequencies correspond to the points at which the stored energy in the system is half of that at resonance (see Figure 3a). The damping ratio is then calculated as it is in the *H-PB*:

$$\lambda = \frac{f_2 - f_1}{2f_r} \quad (1)$$

where λ is the viscous damping ratio, f_r is the resonant frequency, and f_1 and f_2 are the Half-Power frequencies. This method evaluates damping under steady-state harmonic loading conditions and is particularly suitable for small-strain measurements. It implicitly assumes linear damping and a symmetric resonance curve.

In the *F-VD*, the specimen is first excited at or near its resonant frequency. The excitation is abruptly stopped, allowing the system to vibrate freely as its amplitude progressively decays due to energy dissipation within the material. The damping ratio is determined from the logarithmic decrement of successive vibration peaks. If A_n and A_{n+1} are the amplitudes of two successive cycles, the logarithmic decrement δ is defined as:

$$\delta = \ln\left(\frac{A_n}{A_{n+1}}\right) \tag{2}$$

Alternatively, when multiple cycles are considered:

$$\delta = \frac{1}{n}\ln\left(\frac{A_1}{A_{n+1}}\right) \tag{3}$$

where n is the number of cycles between measured amplitudes.

For lightly damped systems ($D < 0.1$), the damping ratio may be approximated as:

$$D = \frac{\delta}{2\pi} \tag{4}$$

For improved accuracy, the expression can be written more rigorously as:

$$D = \frac{1}{\sqrt{4\pi^2 + \delta^2}}\,\delta \tag{5}$$

The *F-VD* method provides a direct quantification of the energy dissipation rate during transient responses and does not depend on the symmetry of the resonance curve. To optimise the response amplitude, *F-VD* tests were conducted at the resonant frequency (f_r) reported in the *H-PB*, under the same confinement and torsional amplitude conditions.

2.3. Experimental Programme Description

For each material, 108 resonant column tests and 108 free-vibration decay tests were carried out. CSS and HDS specimen dimensions were height $h = 100.8$ mm and diameter $d = 49.7$ mm, and CL specimen dimensions were height $h = 109.9$ mm and diameter $d = 49.6$ mm.

The general testing conditions for resonant column tests are summarised in Table 3. Chamber pressure (σ_c), back pressure (B_p), effective confining pressure (σ_c'), and torsional excitation amplitudes (Te) were systematically varied.

Table 3. General conditions for damping assessment by *H-PB* and *F-VD* methods.

σ_c (kPa)	B_p (kPa)	σ_c' (kPa)	Te (V)
450	400	50	0.025, 0.05, 0.1, 0.2, 0.4, 0.8
500	400	100	0.025, 0.05, 0.1, 0.2, 0.4, 0.8
550	400	150	0.025, 0.05, 0.1, 0.2, 0.4, 0.8
600	400	200	0.025, 0.05, 0.1, 0.2, 0.4, 0.8
650	400	250	0.025, 0.05, 0.1, 0.2, 0.4, 0.8
700	400	300	0.025, 0.05, 0.1, 0.2, 0.4, 0.8

While specimen preparation procedures typically adhere to established international standards, the three types of tailings may become unstable during mounting due to their low plasticity. Patiño et al. [19] provide a detailed description of the specimen preparation methods and a series of non-standard accessories designed to ensure the vertical alignment of the excitation head and strict parallelism of the specimen's end surfaces during resonant column testing.

The samples were prepared to a target dry density (γ_d) determined from the homogenised water content (w_h). Using the mould volume and wet density, the required

mass of homogenised material was determined for specimen fabrication. Specimens were prepared to achieve uniform density and moisture distribution prior to installation in the apparatus by the undercompaction moist tamping method [25].

All specimens were saturated with de-aired water by applying an automatic increment of CP and BP under a positive difference of 20 kPa. The increment stopped when a BP of 400 kPa was achieved. This phase lasted over 24 h, ensuring B-values greater than 0.98 due to the complete dissolution of air in the water. B-values confirm the full saturation conditions. After that, the samples were isotropically consolidated under various effective confining stresses (σ_c'): 50, 100, 150, 200, 250, and 300 kPa. Following this, damping assessments were carried out using the *H-PB* and *F-VD* methods.

3. Results and Discussion

Table 4 provides a comprehensive overview of the test results, addressing the measured resonant frequency, angular strain, and damping ratios under all test conditions.

Table 4. Overview of the test results.

		CSS				HDS				CL			
σ_c' (kPa)	Te (V)	f_r (Hz)	γ (%)	λ (%)	D (%)	f_r (Hz)	γ (%)	λ (%)	D (%)	f_r (Hz)	γ (%)	λ (%)	D (%)
50	0.025	50.08	0.004	3.60	3.80	87.20	0.004	1.79	1.37	54.99	0.006	2.99	3.20
50	0.050	50.02	0.008	4.00	4.00	84.33	0.006	2.18	1.81	53.12	0.010	3.61	3.80
50	0.100	47.10	0.017	4.70	4.30	81.00	0.009	2.86	2.47	48.69	0.018	4.12	4.50
50	0.200	43.55	0.033	5.28	4.70	77.77	0.014	3.40	3.21	45.33	0.031	4.61	5.20
50	0.400	38.70	0.065	5.80	5.30	69.59	0.023	4.20	3.90	39.09	0.058	5.32	6.30
50	0.800	27.20	0.148	6.01	6.00	55.97	0.048	5.49	5.83	29.71	0.140	6.91	7.70
100	0.025	64.62	0.003	2.80	3.10	91.20	0.003	1.65	1.49	66.79	0.003	2.25	2.35
100	0.050	61.02	0.006	3.46	3.56	91.27	0.005	2.18	1.85	65.91	0.006	2.80	2.89
100	0.100	58.31	0.011	4.00	3.80	87.07	0.009	2.62	2.37	64.07	0.011	3.40	3.56
100	0.200	52.47	0.024	4.63	4.30	84.09	0.014	3.07	3.20	59.90	0.021	3.80	4.35
100	0.400	47.79	0.048	5.02	4.70	77.66	0.022	3.86	3.90	54.20	0.038	4.65	5.20
100	0.800	40.07	0.096	5.66	5.20	67.91	0.039	5.03	4.70	46.60	0.076	5.32	6.40
150	0.025	71.90	0.004	2.51	2.85	99.76	0.003	1.38	1.50	83.23	0.003	2.18	2.19
150	0.050	69.70	0.008	2.79	3.18	97.60	0.005	2.12	1.76	81.29	0.006	2.43	2.70
150	0.100	67.30	0.013	3.23	3.67	96.50	0.008	2.33	2.12	79.99	0.010	2.78	3.09
150	0.200	63.90	0.022	3.68	3.94	92.20	0.013	2.86	2.91	76.20	0.016	3.24	3.63
150	0.400	59.50	0.038	4.39	4.29	86.02	0.021	3.40	3.64	70.71	0.025	3.71	4.20
150	0.800	52.20	0.064	4.80	4.40	77.10	0.035	4.23	4.50	61.61	0.056	4.31	5.49
200	0.025	76.75	0.004	2.10	2.20	107.88	0.003	1.44	1.26	92.24	0.003	1.73	1.79
200	0.050	77.12	0.008	2.47	2.50	106.00	0.005	1.75	1.59	90.43	0.006	1.98	2.23
200	0.100	74.92	0.013	2.73	2.90	105.00	0.008	2.03	1.92	87.80	0.009	2.42	2.65
200	0.200	71.60	0.022	3.14	3.13	100.21	0.013	2.58	2.58	85.90	0.016	2.71	3.16
200	0.400	67.33	0.037	3.82	3.60	94.32	0.020	3.19	3.05	80.85	0.026	2.98	3.80
200	0.800	61.93	0.062	4.60	3.88	86.03	0.033	3.97	3.85	73.77	0.043	3.29	4.50
250	0.025	84.62	0.004	1.60	1.92	113.12	0.003	1.33	1.23	100.22	0.003	1.73	1.66
250	0.050	82.30	0.007	2.00	2.31	112.00	0.005	1.66	1.55	97.62	0.005	1.91	2.00
250	0.100	81.20	0.013	2.34	2.46	110.00	0.008	2.09	2.02	94.90	0.009	2.29	2.52
250	0.200	78.30	0.022	2.74	2.79	106.00	0.012	2.42	2.59	93.10	0.015	2.53	2.99
250	0.400	74.50	0.036	3.35	3.24	100.19	0.019	3.06	3.10	88.10	0.025	2.91	3.68
250	0.800	69.00	0.058	3.91	3.78	92.20	0.031	3.75	3.59	81.33	0.041	3.43	4.27
300	0.025	88.77	0.004	1.40	1.70	118.33	0.003	1.19	1.15	107.88	0.003	1.32	1.36
300	0.050	89.60	0.007	1.61	1.84	117.00	0.005	1.71	1.60	106.79	0.005	1.75	2.03
300	0.100	87.50	0.012	2.10	2.27	115.41	0.007	1.97	1.80	104.00	0.009	1.88	2.40
300	0.200	86.00	0.021	2.43	2.50	111.89	0.011	2.25	2.10	102.00	0.015	2.12	2.76
300	0.400	82.00	0.034	2.90	2.82	105.79	0.018	2.78	2.60	97.20	0.024	2.38	3.37
300	0.800	75.88	0.050	3.60	3.38	98.55	0.028	3.61	3.40	90.68	0.035	2.79	4.01

3.1. Results of Damping Ratio from Half-Power Bandwidth Method

The hysteretic damping ratio values reported in Table 4 and plotted in Figure 4 were obtained from forced-vibration measurements in resonant column mode using the Half-Power Bandwidth (*H-PB*) method. Figure 4 presents, for each material, the variation in λ with cyclic angular strain γ at different effective consolidation pressures (σ'_c). The results indicate that, across all materials, the effective consolidation pressure clearly influences $\lambda(\gamma)$. Hence, at a given strain level, λ decreases markedly with increasing σ'_c. In addition, for all materials and confinement levels, λ generally increases with increasing γ. The strain dependency is more pronounced at lower σ'_c. For example, at $\gamma = 0.04\%$, increasing σ'_c from 50 to 300 kPa reduces the absolute λ values by 2.3% (CSS), 1.5% (HDS), and 2.6% (CL).

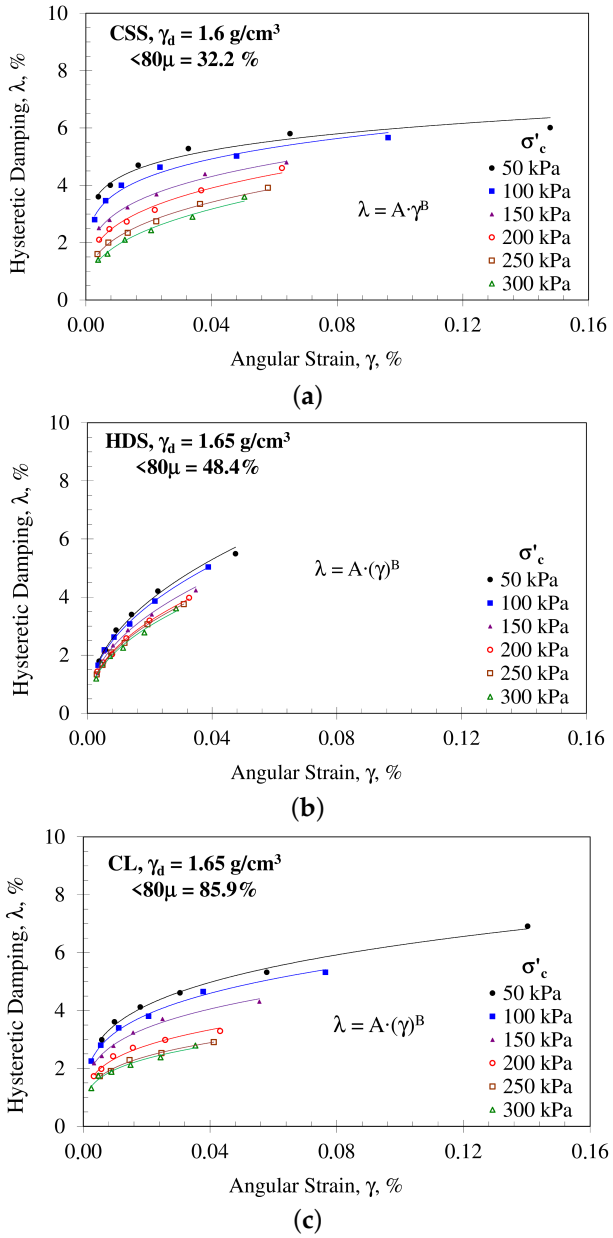


Figure 4. Variation trends in the damping ratio by the *H-PB* method as a function of the angular strain, for different effective consolidation pressures: (**a**) CSS tailing; (**b**) HDS tailing; (**c**) CL tailing.

For modelling purposes, the relationship between hysteretic damping ratio and cyclic angular strain may be approximated, for each material and each effective consolidation pressure level, by a power-law expression:

$$\lambda = A\,\gamma^{B} \tag{6}$$

where λ is the hysteretic damping ratio, γ is the cyclic angular strain, and A and B are empirical constants. The fitted values of A and B for each material and σ_c' are reported in Table 5.

Table 5. Empirical constants of Equations (6) and (10).

	CSS				HDS				CL			
σ_c' (kPa)	*A*	*B*	*C*	*E*	*A*	*B*	*C*	*E*	*A*	*B*	*C*	*E*
50	8.48	0.15	7.49	0.13	22.43	0.45	34.19	0.57	11.20	0.25	13.59	0.28
100	9.22	0.20	7.32	0.14	21.39	0.45	24.93	0.49	10.38	0.25	13.68	0.30
150	9.57	0.25	7.22	0.17	19.38	0.44	23.77	0.49	9.20	0.25	13.91	0.32
200	9.82	0.29	7.15	0.21	17.95	0.44	20.68	0.49	7.59	0.26	13.98	0.36
250	9.61	0.32	7.11	0.24	17.53	0.44	17.53	0.44	6.58	0.26	14.10	0.37
300	10.27	0.37	7.11	0.26	16.96	0.44	15.50	0.44	6.37	0.26	14.12	0.38

To generalise Equation (6), the parameters A and B were expressed as functions of effective consolidation pressure using power-law relationships:

$$A = I\,(\sigma_c')^{J} \tag{7}$$

$$B = K\,(\sigma_c')^{L} \tag{8}$$

as illustrated in Figures 5 and 6. Substitution of Equations (7) and (8) into Equation (6) yields the general expression:

$$\lambda = I\,(\sigma_c')^{J}\,\gamma^{K(\sigma_c')^{L}} \tag{9}$$

where I, J, K and L are empirical constants (Table 6).

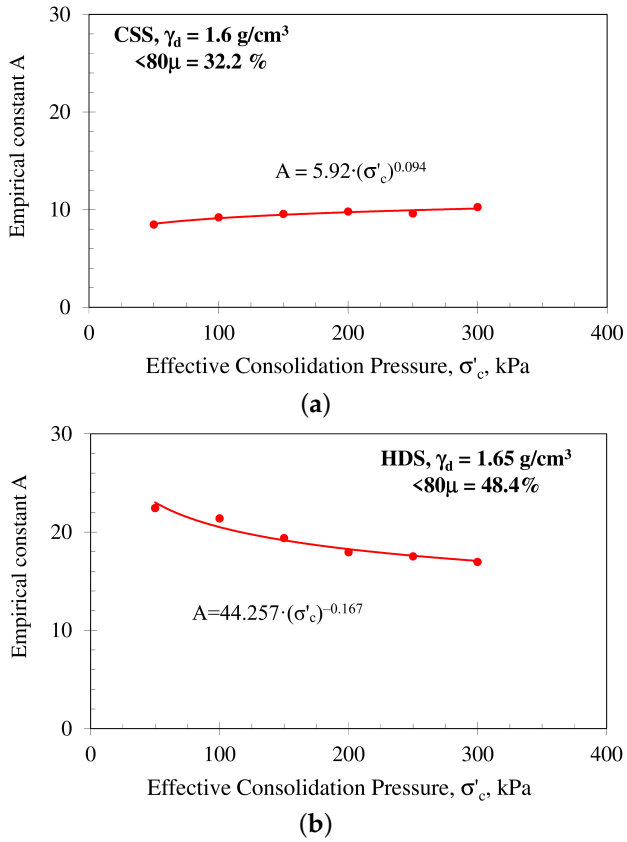
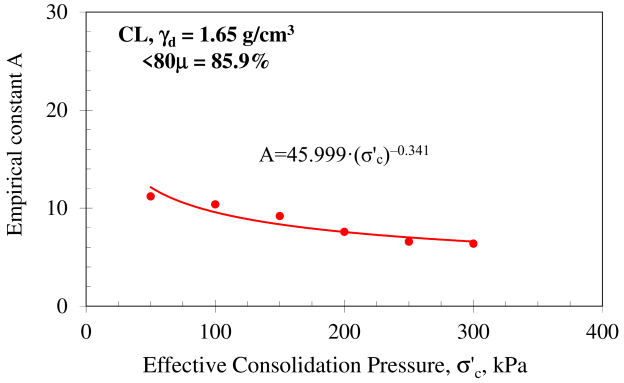
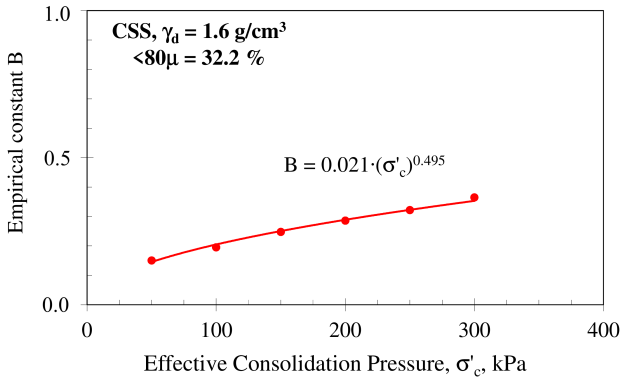


Figure 5. *Cont.*

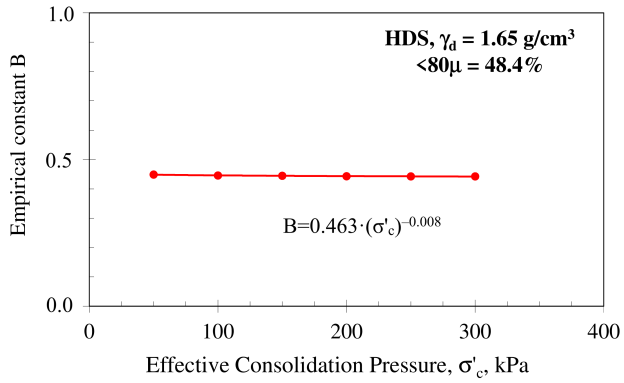


(**c**)

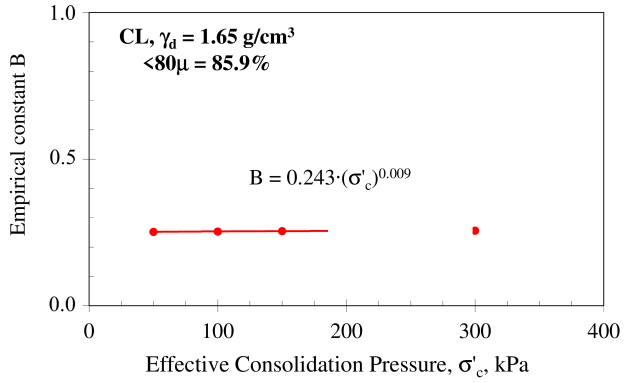
Figure 5. Variation trends in the empirical constant *A* with the confinement: (**a**) CSS tailing; (**b**) HDS tailing; (**c**) CL tailing.



(**a**)



(**b**)



(**c**)

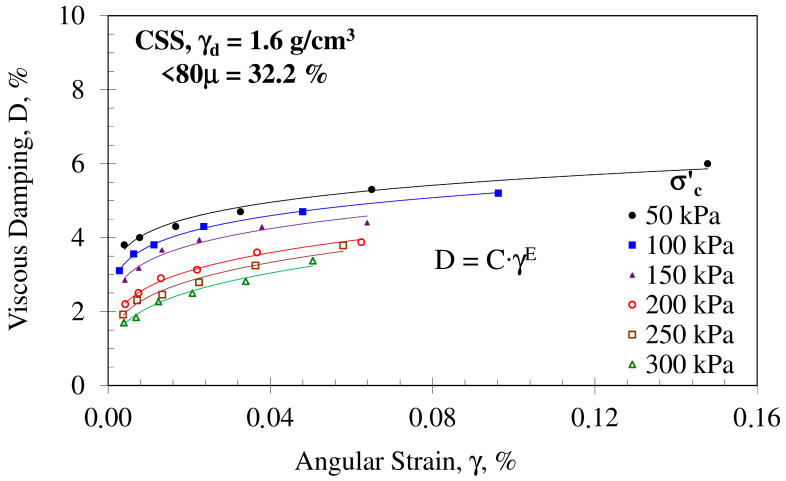
Figure 6. Variation trends in the empirical constant *B* with the confinement: (**a**) CSS tailing; (**b**) HDS tailing; (**c**) CL tailing.

Table 6. Empirical constants of Equations (9) and (13).

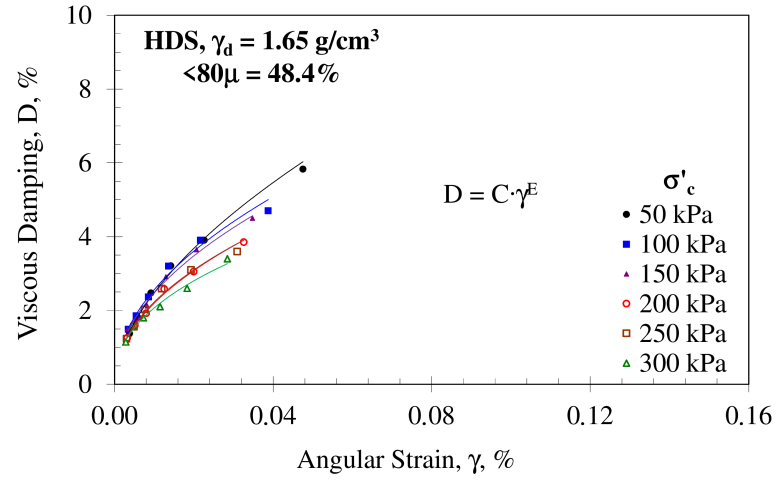
Material	λ Formulation				D Formulation			
	I	***J***	***K***	***L***	***M***	***N***	***O***	***P***
CSS	5.92	0.094	0.021	0.495	8.44	−0.031	0.023	0.415
HDS	44.26	−0.167	0.463	−0.008	176.20	−0.415	0.965	−0.137
CL	46.00	−0.341	0.243	0.009	12.38	0.023	0.130	0.187

3.2. Results of Damping Ratio from Free-Vibration Decay Method

To complement the hysteretic damping analysis, the viscous damping ratio values (D) reported in Table 4 and plotted in Figure 7 were obtained from the decay of free vibrations using the free-vibration decay (*F-VD*) method. Figure 7 shows the variation in D with cyclic angular strain γ at different effective consolidation pressures σ_c'. From this figure, it can be observed that for all materials and confinement levels, D generally increases with increasing γ. In addition, at a given strain level, D exhibits systematic variation with σ_c', consistent with the confinement dependency observed for λ.

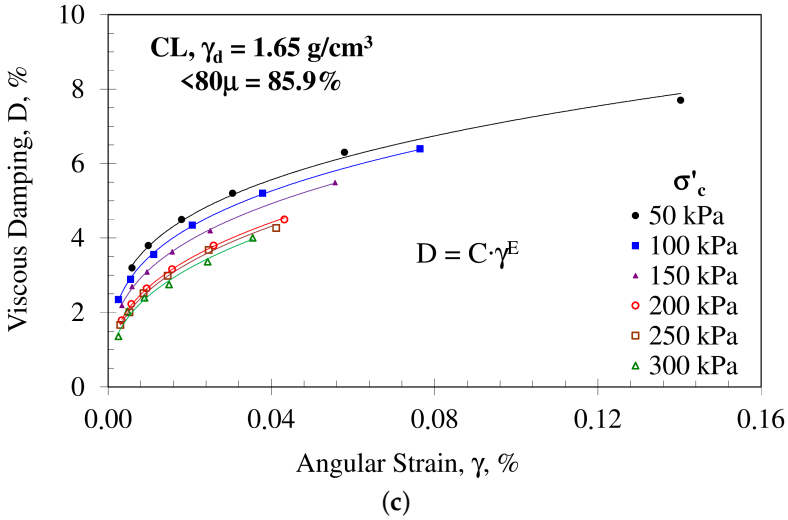


(**a**)



(**b**)

Figure 7. *Cont.*



(**c**)

Figure 7. Variation trends in the damping ratio by the *F-VD* method as a function of the angular strain, for different effective consolidation pressures: (**a**) CSS tailing; (**b**) HDS tailing; (**c**) CL tailing.

For modelling purposes, the dependence of viscous damping ratio on cyclic angular strain may be approximated by:

$$D = C\,\gamma^{E} \tag{10}$$

where C and E are empirical constants (Table 5). To generalise Equation (10), the parameters C and E were expressed as functions of effective consolidation pressure:

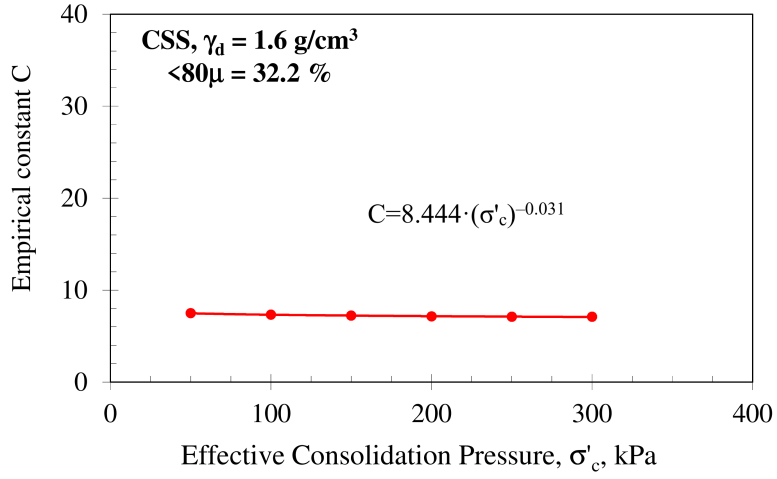
$$C = M\,(\sigma_c')^{N} \tag{11}$$

$$E = O\,(\sigma_c')^{P} \tag{12}$$

as shown in Figures 8 and 9. Combining Equations (10)–(12) provides:

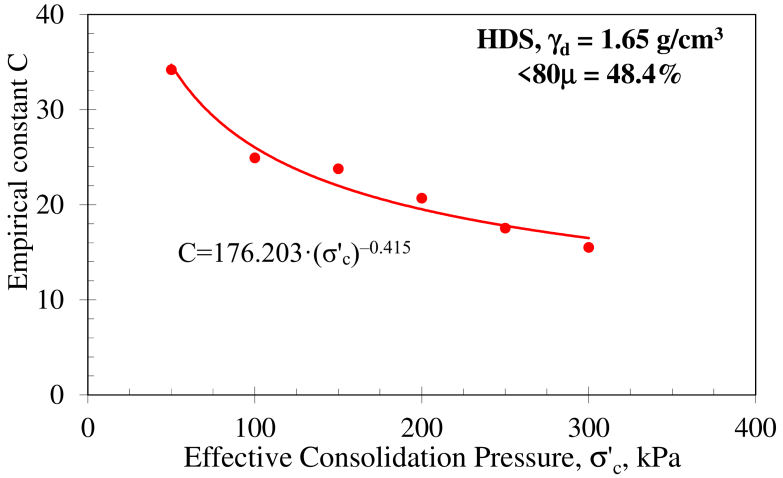
$$D = M\,(\sigma_c')^{N}\,\gamma^{O(\sigma_c')^{P}} \tag{13}$$

where M, N, O and P are empirical constants (Table 6).

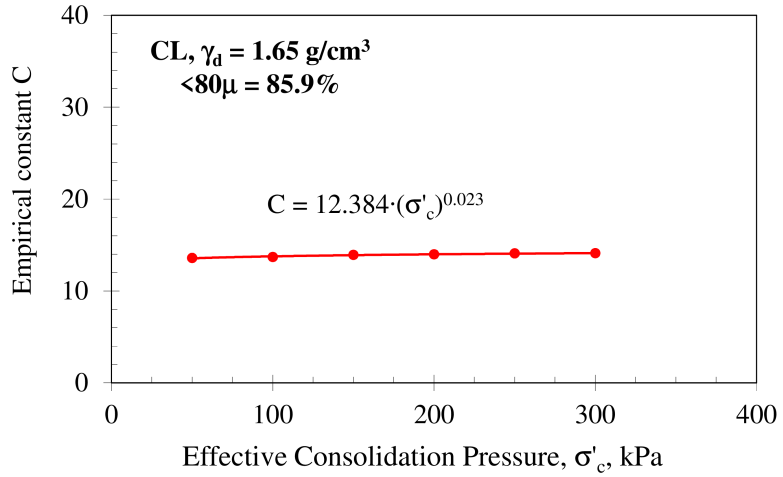


(**a**)

Figure 8. *Cont.*

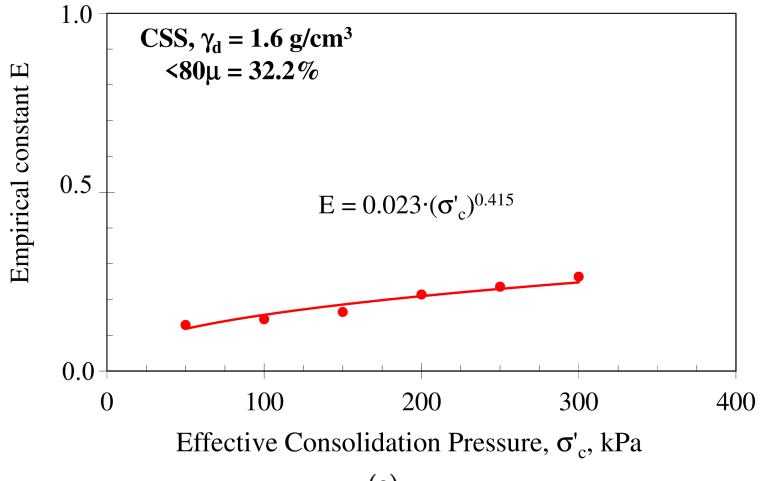


(**b**)



(**c**)

Figure 8. Variation trends in the empirical constant *C* with the confinement: (**a**) CSS tailing; (**b**) HDS tailing; (**c**) CL tailing.



(**a**)

Figure 9. *Cont.*

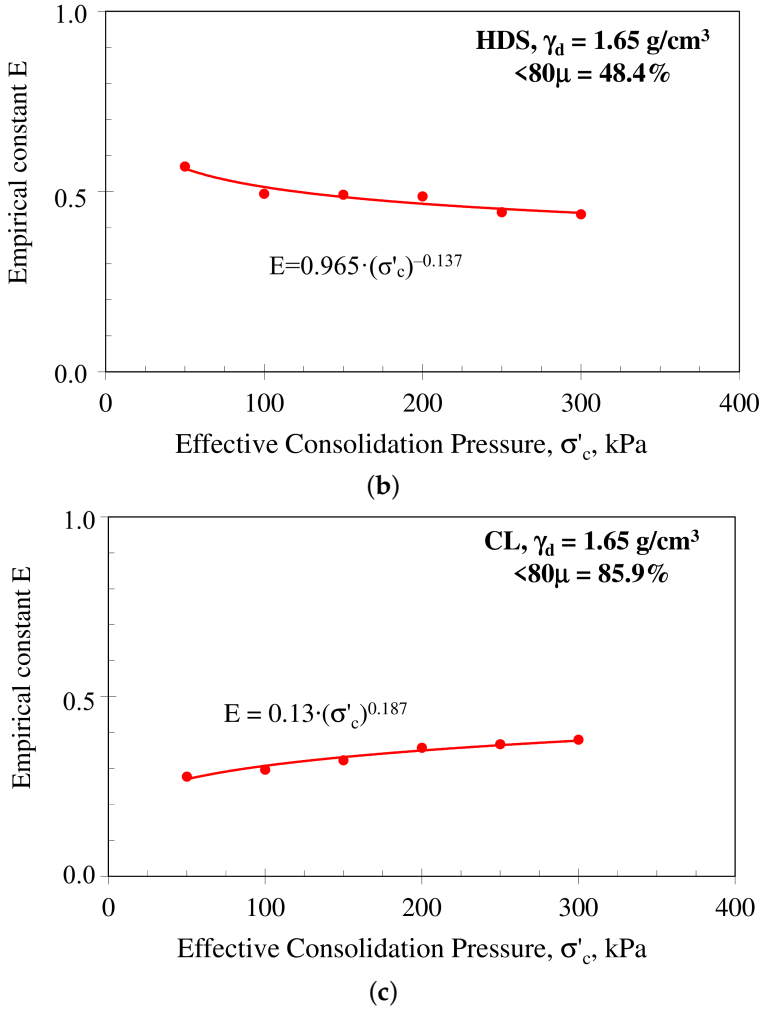


Figure 9. Variation trends in the empirical constant *E* with the confinement: (**a**) CSS tailing; (**b**) HDS tailing; (**c**) CL tailing.

3.3. Relationship Between Viscous and Hysteretic Damping

In addition to the empirical functions relating damping ratios to strain and effective consolidation pressure (Equations (9) and (13)), a key outcome of this study is the establishment of relationships between the two damping descriptors, D and λ. Figure 10 presents the variation in D as a function of λ for each material at different σ_c' values.

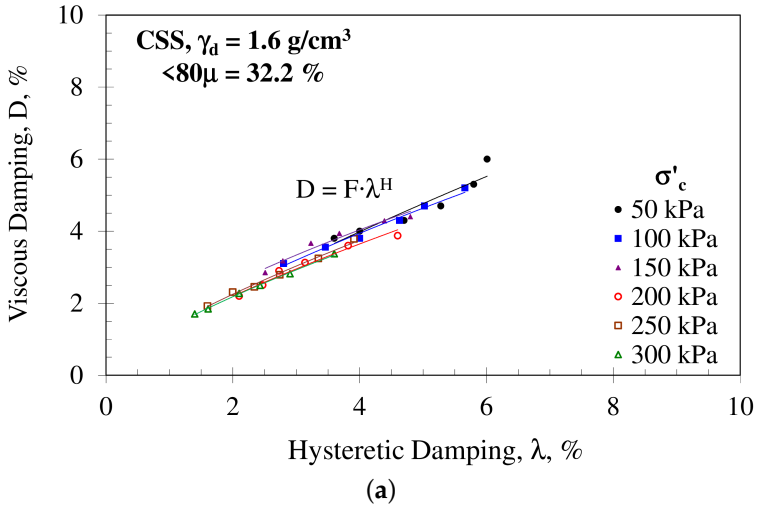


Figure 10. *Cont.*

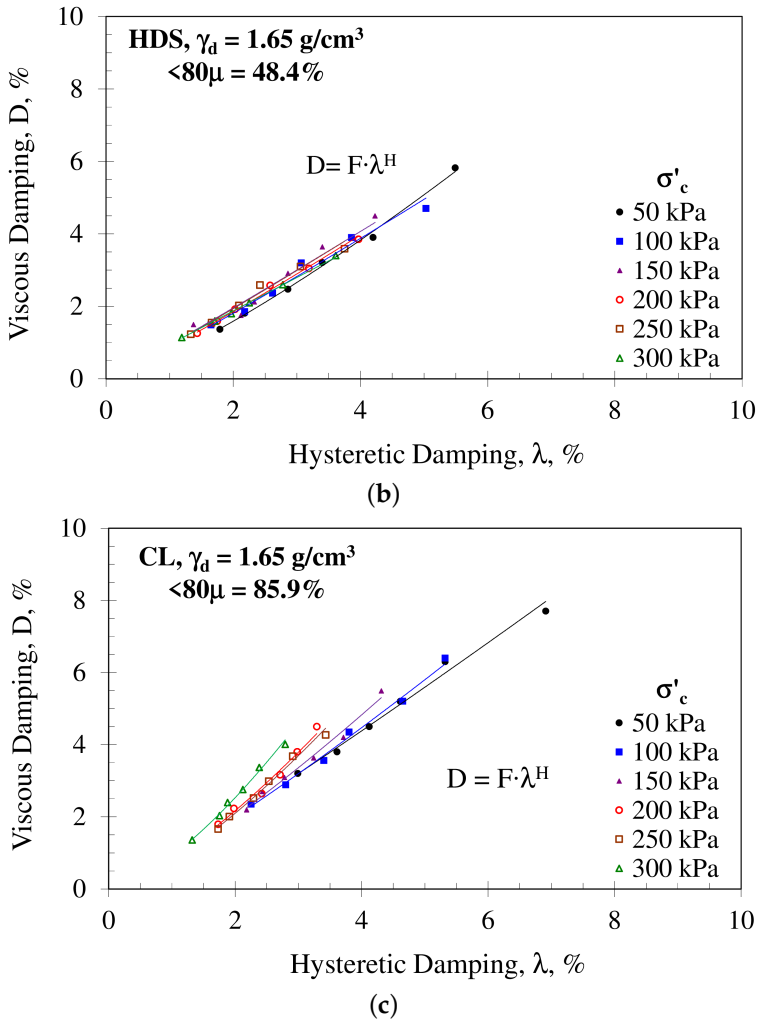


Figure 10. Variation between λ and D under different effective consolidation pressure: (**a**) CSS tailing; (**b**) HDS tailing; (**c**) CL tailing.

For modelling purposes, for each material and effective consolidation pressure level, the relationship may be approximated by:

$$D = F\,\lambda^{H} \tag{14}$$

where F and H are empirical constants (Table 7). To generalise Equation (14), the parameters were related to effective consolidation pressure using:

$$F = Q\,(\sigma_c')^{R} \tag{15}$$

$$H = S\,(\sigma_c')^{T} \tag{16}$$

as shown in Figures 11 and 12. Substituting Equations (15) and (16) into Equation (14) yields:

$$D = Q\,(\sigma_c')^{R}\,\lambda^{S(\sigma_c')^{T}} \tag{17}$$

where Q, R, S and T are empirical constants (Table 8).

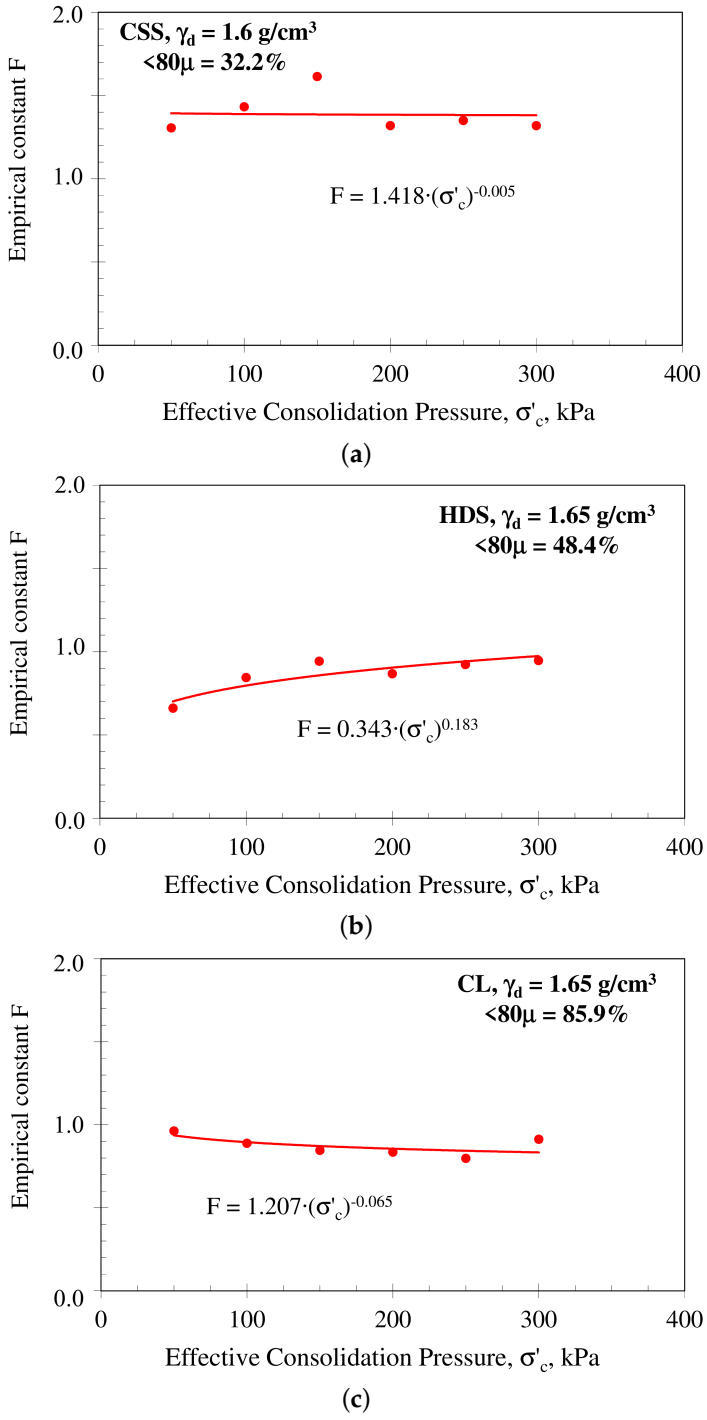


Figure 11. Variation trends in the empirical constant *F* with the confinement: (**a**) CSS tailing; (**b**) HDS tailing; (**c**) CL tailing.

Table 7. Empirical constants of Equation (14).

	CSS		HDS		CL	
σ_c' (kPa)	*F*	*H*	*F*	*H*	*F*	*H*
50	1.31	0.80	0.66	1.27	0.96	1.09
100	1.43	0.73	0.84	1.10	0.89	1.17
150	1.61	0.66	0.94	1.05	0.85	1.26
200	1.32	0.73	0.87	1.10	0.84	1.38
250	1.35	0.74	0.92	1.07	0.80	1.40
300	1.32	0.72	0.95	0.99	0.91	1.47

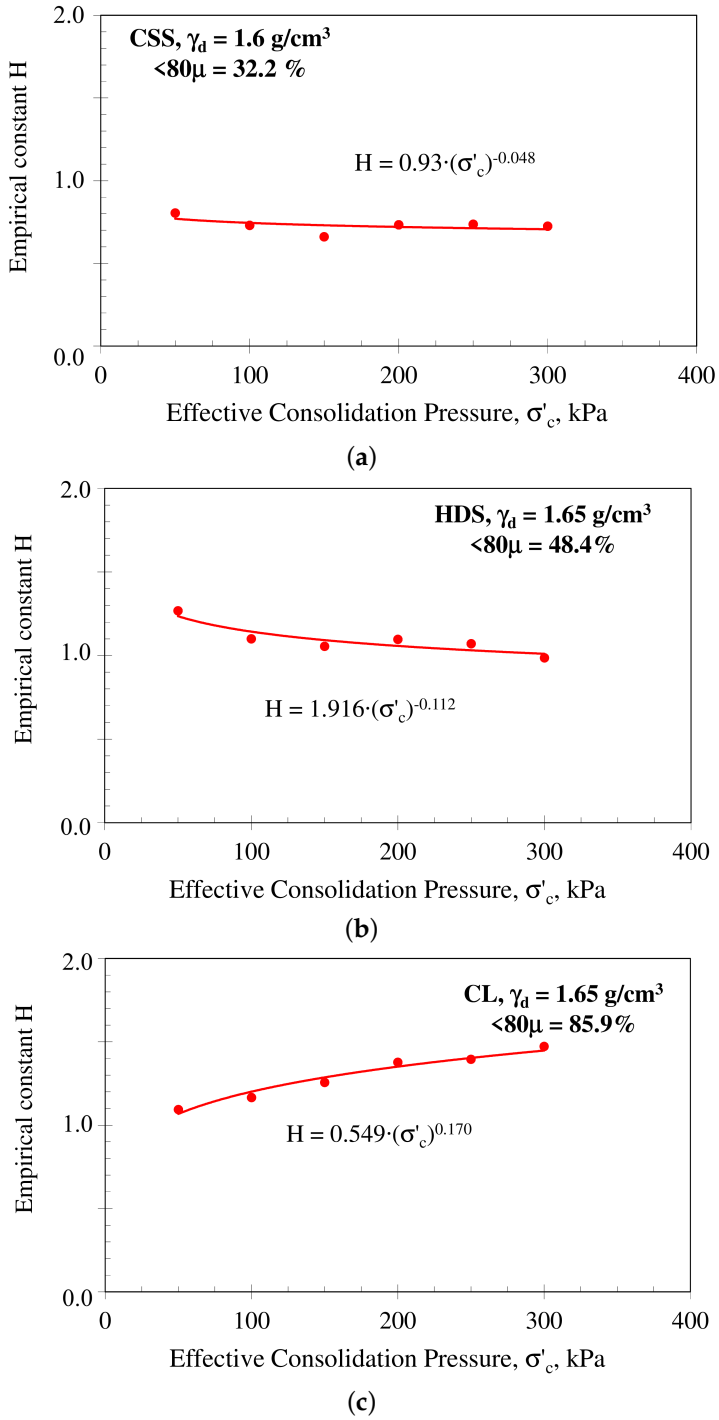


Figure 12. Variation trends in the empirical constant H with the confinement: (**a**) CSS tailing; (**b**) HDS tailing; (**c**) CL tailing.

To maximise practical use of the experimental dataset, Figure 13 presents the overall D–λ relationship for each material using all results, without discretisation by γ or σ_c'. This figure indicates that for the predominantly granular materials (i.e., CSS and HDS), D tends to be close to λ. For CSS, a small deviation is observed: for $\lambda < 4$, D is slightly larger than λ, whereas for $\lambda > 4$, D is slightly smaller. For practical purposes, $D \approx \lambda$ may be adopted for CSS and HDS within the tested ranges. For the tailings with plastic fines (CL), D is generally greater than λ.

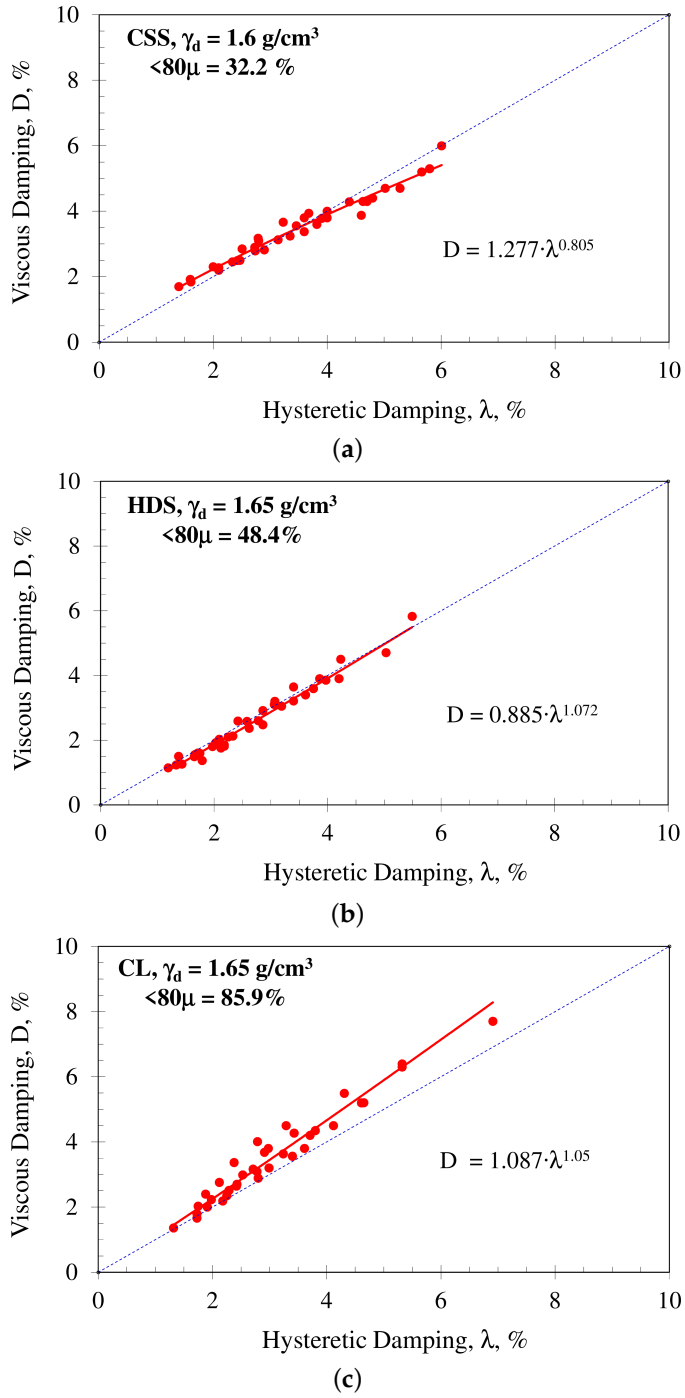


Figure 13. Variation trends between λ and D: (**a**) CSS tailing; (**b**) HDS tailing; (**c**) CL tailing.

Although Equation (17) explicitly accounts for the effect of σ_c', the clustering of all results suggests that a simplified global relationship may be adopted:

$$D = U\,\lambda^V \tag{18}$$

where U and V are empirical constants (Table 8). It should be noted that, in general, D depends not only on λ but also on γ and σ_c'; however, the (D, λ) pairs occupy different regions of Figure 10 while still following the trend described by Equation (18).

Table 8. Empirical constants of Equations (17) and (18).

Material	Generalised Formulation				Simplified Formulation	
	Q	***R***	***S***	***T***	***U***	***V***
CSS	1.418	−0.005	0.930	−0.048	1.277	0.805
HDS	0.343	0.183	1.916	−0.112	0.885	1.072
CL	1.207	−0.065	0.549	0.170	1.087	1.050

3.4. Interpretation and Discussion of the Relationship Between Damping Estimation Methods

Beyond the empirical correlations established in this study, it is important to provide a physical interpretation of the observed relationships between hysteretic damping (λ) and viscous damping (D), particularly in light of the distinct behaviours exhibited by granular (CSS and HDS) and cohesive (CL) materials.

For the predominantly granular materials (CSS and HDS), the results indicate that $D \approx \lambda$ over most of the investigated strain and confinement ranges. This suggests that, under the tested conditions, the viscous damping obtained from free-vibration decay closely approximates the energy dissipated through hysteretic mechanisms during forced vibration. In clean or low-plasticity granular soils, energy dissipation is primarily governed by frictional sliding at particle contacts and minor rearrangement of the soil skeleton. These mechanisms are strain-dependent but exhibit limited time dependence over the frequency range considered (28–118 Hz). Consequently, the viscous damping derived from transient decay provides a consistent approximation of the energy loss per cycle.

In contrast, the cohesive material (CL), characterised by a significant proportion of phyllosilicates and measurable plasticity (PI = 7%), consistently exhibited $D > \lambda$. This behaviour may be attributed to the combined influence of interparticle bonding, physico-chemical interactions and internal viscous resistance within the clay matrix. These processes introduce additional time-dependent components into the material response, which are better captured by the free-vibration decay method. As a result, the viscous damping ratio tends to exceed the hysteretic damping estimated from the resonance curve.

The role of effective consolidation pressure further supports this interpretation. Increasing σ_c' leads to reduced damping in all materials, reflecting the stabilisation of the soil skeleton and the restriction of interparticle slip [14,18,26]. At higher confinement levels, contact stiffness increases and micro-sliding mechanisms become less pronounced, resulting in lower energy dissipation [16,24]. In cohesive material, higher confinement also reduces the contribution of fabric-related rearrangements, although time-dependent mechanisms remain active, which may explain the persistence of $D > \lambda$.

The frequency range employed in resonant column testing may also contribute to the observed differences. The forced-vibration response (Half-Power method) is determined at steady-state resonance, whereas the free-vibration decay method captures transient behaviour immediately after excitation removal [20]. If the material exhibits even moderate viscoelastic behaviour, the decay response may include additional damping contributions due to rate effects. This influence is expected to be more significant in materials with higher fines content and greater physico-chemical activity, such as CL.

From a microstructural perspective, the quartz-dominated CSS and HDS materials behave primarily as frictional granular assemblies, where damping is controlled by contact mechanics [24]. Conversely, the mineralogical composition of CL, which includes phyllosilicates and metallic minerals, promotes a more complex interaction network involving particle-to-particle bonding, internal shear within clay platelets and fluid-mediated dis-

sipation. This structural difference provides a consistent explanation for the systematic deviation of CL results from the $D = \lambda$ line.

Overall, the findings indicate that the equivalence between hysteretic and viscous damping in soils is not universal but depends on soil type, mineralogical composition and stress state. The proposed empirical relationships therefore provide not only practical predictive tools but also insight into the underlying mechanisms governing energy dissipation in different geomaterials.

4. Conclusions

This study investigated the damping ratio of three tailings materials obtained from the Riotinto mining district (Huelva, Spain), identified as Cerro Salomón Sand (CSS), High-Density Sludge (HDS) and Copper Lamas (CL), by comparing two experimental methods. The conclusions are supported by identification and classification tests, with 108 resonant column tests and 108 free-vibration decay tests performed under effective consolidation pressures ranging from 50 to 300 kPa.

The main findings of this research are summarised as follows:

- CSS and HDS behave as predominantly granular, non-plastic materials with high fines content, whereas CL is classified as a low-plasticity clay. The three materials exhibit unusually high specific gravities due to the heavy minerals associated with the mining process.
- For the three tailings materials, both the hysteretic damping ratio (λ) and viscous damping ratio (D) increase with increasing cyclic angular strain (γ), confirming the strong strain dependency of energy dissipation mechanisms.
- At a given strain level, both λ and D decrease systematically with increasing effective consolidation pressure (σ'_c), indicating that confinement stabilises the soil skeleton and reduces interparticle energy dissipation.
- The strain dependency of damping is more pronounced at lower confinement levels, suggesting that micro-sliding and structural rearrangement mechanisms are progressively inhibited as σ'_c increases.
- Power-law relationships provide accurate representations of the variation of λ and D with γ for each confinement level. Furthermore, the empirical constants governing these expressions can themselves be expressed as functions of σ'_c, enabling generalised formulations that reproduce experimental behaviour over wide strain and stress ranges.
- A key contribution of this research is the establishment of direct empirical relationships between viscous and hysteretic damping ratios. For the granular materials (CSS and HDS), D is approximately equal to λ within the investigated ranges, whereas for the cohesive material (CL), D is generally greater than λ. This distinction reflects the different energy dissipation mechanisms governing granular and cohesive soils.
- The simplified potential-type relationship $D = U\lambda^V$ provides a practical and robust approximation of the interaction between the two damping descriptors. Although both D and λ depend on γ and σ'_c, the (D, λ) pairs follow a consistent mathematical trend, allowing direct estimation of one parameter from the other for the materials studied.
- The proposed empirical formulations reproduce the experimental results with good accuracy and may significantly reduce the number of laboratory tests required for characterisation. In practical terms, reliable damping estimates can be obtained using a limited number of torsional excitation levels and effective consolidation pressures.
- From an engineering perspective, the methodology presented herein provides a rational and simplified framework for incorporating damping behaviour into numerical

simulations and dynamic analyses, particularly when distinguishing between two experimental methods.

Overall, the results demonstrate that the relationship between viscous and hysteretic damping in soils is soil-type-dependent and influenced by stress state and strain level. The proposed empirical functions offer both practical predictive capability and insight into the mechanisms governing energy dissipation in mining tailings materials. The findings presented here are based on small to medium strain levels typical of resonant column testing; additional studies at larger strains are necessary to explore other conditions and enhance these results.

Author Contributions: Conceptualisation, H.P.; methodology, H.P.; software, H.P. and R.Á.G.-A.; validation, R.Á.G.-A. and F.M.-G.; formal analysis, H.P., R.Á.G.-A. and F.M.-G.; investigation, H.P.; resources, H.P.; data curation, H.P.; writing—original draft preparation, H.P.; writing—review and editing, R.Á.G.-A. and F.M.-G.; visualisation, R.Á.G.-A. and F.M.-G.; supervision, R.Á.G.-A. and F.M.-G.; project administration, H.P.; funding acquisition, H.P. All authors have read and agreed to the published version of the manuscript.

Funding: This publication is part of the project PID2022-139202OB-I00, Neural networks and optimization techniques for the safe design and maintenance of transport infrastructure: volcanic rock geotechnics and Slope Stability (IA-Pyroslope), funded by the State Research Agency of the Ministry of Science, Innovation and Universities and the European Regional Development Fund, MCIN/AEI/10.13039/501100011033/ERDF, EU.

Data Availability Statement: Data generated or analysed during this study are available from the corresponding author upon reasonable request.

Acknowledgments: The authors would like to express their gratitude to the José Entrecanales Ibarra Foundation for donating the essential equipment for this research, particularly the resonant column. The support of EPTISA Engineering Services for sponsoring the research through an agreement with the Agustín de Betancourt Foundation is also acknowledged. Additionally, they are grateful to the UPM for its unwavering support of experimental research, especially to the late Antonio Soriano.

Conflicts of Interest: The authors declare no conflicts of interest.

References

1. Hardin, B.O.; Drnevich, V.P. Shear modulus and damping in soils: Measurement and parameter effects. *J. Soil Mech. Found. Div. ASCE* **1972**, *98*, 603–624. [CrossRef]
2. Hardin, B.O.; Drnevich, V.P. Shear modulus and damping in soils: Design equations and curves. *J. Soil Mech. Found. Div. ASCE* **1972**, *98*, 667–692. [CrossRef]
3. Seed, H.B.; Idriss, I.M. *Soil Moduli and Damping Factors for Dynamic Response Analyses*; Report EERC 70-10; University of California: Berkele, CA, USA, 1970.
4. Vucetic, M.; Dobry, R. Effect of soil plasticity on cyclic response. *J. Geotech. Eng.* **1991**, *117*, 89–107. [CrossRef]
5. Vucetic, M.; Lanzo, G.; Doroudian, M. Damping at Small Strains in Cyclic Simple Shear Test. *J. Geotech. Geoenviron. Eng.* **1998**, *124*, 585–594. [CrossRef]
6. Zergoun, M.; Vaid, Y.P. Effective stress response of clay to undrained cyclic loading. *Can. Geotech. J.* **1994**, *31*, 714–727. [CrossRef]
7. Brennan, A.J.; Thusyanthan, N.I.; Madabhushi, S.P.G. Evaluation of shear modulus and damping in dynamic centrifuge test. *J. Geotech. Geoenviron. Eng.* **2005**, *131*, 1488–1498. [CrossRef]
8. Soriano, A.; Patiño, H.; González, J.; Valderrama, M. Cyclic behaviour of saturated sands subject to previous horizontal shear stresses. In *Proceedings of the 15th European Conference on Soil Mechanics and Geotechnical Engineering, Athens, Greece, 14 September 2011*; IOS Press: Amsterdam, The Netherlands, 2011. [CrossRef]
9. Patiño, H.; Galindo, R. Damping of a soft marine clay subjected to the combination of monotonic and cyclic shear stresses. *Eur. J. Environ. Civ. Eng.* **2021**, *27*, 72–95. [CrossRef]
10. Kuribayashi, E.; Iwasaki, T.; Tatsuoka, F. Effects of stress-strain conditions on dynamic properties of sands. *Proc. JSCE* **1975**, *242*, 105–114. [CrossRef]

11. Senetakis, K.; Anastasiadis, A.; Pitilakis, K. The Small-Strain Shear Modulus and Damping Ratio of Quartz and Volcanic Sands. *Geotech. Test. J.* **2012**, *35*, 20120073. [CrossRef]
12. Zhang, J.; Andrus, R.D.; Juang, C.H. Normalized shear modulus and material damping ratio relationships. *J. Geotech. Geoenviron. Eng.* **2005**, *131*, 453–464. [CrossRef]
13. Wichtmann, T.; Triantafyllidis, T. Effect of Uniformity Coefficient on G/Gmax and Damping Ratio of Uniform to Well-Graded Quartz Sands. *J. Geotech. Geoenviron. Eng.* **2013**, *139*, 59–72. [CrossRef]
14. Ham, A.; Wang, J.; Stammer, J.G. Relationships between Particle Shape Characteristics and Macroscopic Damping in Dry Sands. *J. Geotech. Geoenviron. Eng.* **2012**, *138*, 1002–1011. [CrossRef]
15. Madhusudhan, B.N.; Kumar, J. Damping of Sands for Varying Saturation. *J. Geotech. Geoenviron. Eng.* **2013**, *139*, 107–116. [CrossRef]
16. Subramaniam, P.; Banerjee, S.; Ku, T. Shear Modulus and Damping Ratio Model for Cement Treated Clay. *Int. J. Geomech.* **2019**, *19*, 06019010. . [CrossRef]
17. Rollins, K.M.; Singh, M.; Roy, J. Simplified Equations for Shear-Modulus Degradation and Damping of Gravels. *J. Geotech. Geoenviron. Eng.* **2020**, *146*, 04020076. [CrossRef]
18. Molina-Gómez, F.; Viana da Fonseca, A.; Ferreira, C.; Camacho-Tauta, J. Dynamic properties of two historically liquefiable sands in the Lisbon area. *Soil Dyn. Earthq. Eng.* **2020**, *132*, 106101. [CrossRef]
19. Patiño, H.; Molina-Gómez, F.; Galindo, R.; Viana da Fonseca, A. Integrated evaluation of stiffness degradation by combining Resonant-Column, Cyclic Triaxial and Cyclic Simple Shear Tests: Application to Riotinto mine tailings. *Geomech. Energy Environ.* **2025**, *41*, 100652. [CrossRef]
20. Schaeffer, K.; Bearce, R.; Wang, J. Dynamic Modulus and Damping Ratio Measurements from Free-Free Resonance and Fixed-Free. *Geotech. Geoenviron. Eng.* **2013**, *139*, 2145–2155. [CrossRef]
21. Senetakis, K.; Anastasiadis, A.; Pitilakis, K. A comparison of material damping measurements in resonant column using the steady-state and free-vibration decay methods. *Soil Dyn. Earthq. Eng.* **2015**, *74*, 10–13. [CrossRef]
22. Xu, Z.; Tao, Y.; Hernandez, L. Novel methods for the computation of small-strain damping ratios of soils from cyclic torsional shear and free-vibration decay testing. *Geotechnics* **2021**, *1*, 330–346. [CrossRef]
23. Mog, K.; Anbazhagan, P. Evaluation of the damping ratio of soils in a resonant column using different methods. *Soils Found.* **2022**, *62*, 101091. [CrossRef]
24. Patiño, H.; Molina-Gómez, F.; Galindo, R.; Viana da Fonseca, A. Stiffness degradation of non-plastic copper ore tailings. *GéOtechnique Lett.* **2025**, *15*, 219–225. [CrossRef]
25. Lade, P.V. *Triaxial Testing of Soils*, 1st ed.; John Wiley & Sons, Ltd.: Chichester, UK, 2016.
26. Caicedo, B.; Chaparro, M.J.; Castillo Betancourt, J.P.; Cabrera, M.A.; Delage, P.; LognonnÉ, P.H.; Banerdt, B. A micromechanical model for estimating the shear modulus and damping ratio of loose sands under low stresses: Application to a Mars regolith simulant. *Géotechnique* **2025**, *75*, 379–392. [CrossRef]

Disclaimer/Publisher's Note: The statements, opinions and data contained in all publications are solely those of the individual author(s) and contributor(s) and not of MDPI and/or the editor(s). MDPI and/or the editor(s) disclaim responsibility for any injury to people or property resulting from any ideas, methods, instructions or products referred to in the content.